Numerical study of turbulent flow and heat transfer of nanofluids in pipes

Hendrik Boertz[a], Albert Baars[a], Janusz T. Cieslinski[b], Slawomir Smolen[a]

[a]City University of Applied Sciences Bremen, Bremen, Germany

[b]Gdansk University of Technology, Gdańsk, Poland

Address correspondence to Professor Janusz T. Cieśliński, Faculty of Mechanical Engineering, Gdansk University of Technology, 11/12 Narutowicza, 80-233, Gdansk/Poland, Telephone: +48 583471622, Fax: +48 583472816, E-mail: jcieslin@pg.gda.pl

Keywords: Nanofluids, Turbulent flow, Heat transfer enhancement, Friction factor

ABSTRACT

In this work, Nusselt number and friction factor are calculated numerically for turbulent pipe flow (Reynolds number between 6000 and 12000) with constant heat flux boundary condition using nanofluids. The nanofluid is modelled with the single-phase approach and the simulation results are compared with correlations from experimental data. Ethylene glycol and water, 60:40 EG/W mass ratio, as base fluid and SiO_2 nanoparticles are used as nanofluid with particle volume concentrations ranging from 0% to 10%. Nusselt number predictions for the nanofluid are in agreement with experimental results and a conventional single-phase correlation. The mean deviation is in the range of -5%. Friction factor values show a mean deviation of 0.5% to a conventional single-phase correlation, however, they differ considerably from the nanofluid experimental data. The results indicate that the nanofluid requires more pumping power than the base fluid for high particle concentrations and Reynolds numbers on the basis of equal heat transfer rate.

3

INTRODUCTION

Nanofluids are two-phase mixtures of conventional heat transfer fluids and solid particles of sizes below 100 nm which were first defined by Choi and Eastman [1] in 1995. This group of fluids provides enhanced heat transfer compared to conventional fluids, which is partially due to the increase in thermal conductivity and also the reduction of thermal boundary layer thickness caused by the presence of particles and their random motion within the base fluid [2]. Especially the thermal conductivity enhancement is not yet understood, as there is no reliable theory to predict the anomalous thermal transport of nanofluids [3]. Nanofluid research is becoming important as thermal loads are increasing and applications sizes are decreasing while heat transfer efficiency maximization has reached the limits by using the optimal conventional heat transfer fluid and extended surfaces [4, 5]. Kulkarni et al. [6] mentioned that nanofluids may reduce volumetric and mass flow rates and this results in an overall pumping power saving. Furthermore, heat transfer applications can be built more compact. Therefore nanofluids can be used for a variety of applications [7], e.g. heating buildings [6], cooling system for wind turbines [8] and solar absorption [9–11].

There are basically two approaches to model heat transfer and flow behaviour of nanofluids. The first assumes that liquid and solid phase are in thermal equilibrium with zero relative velocity [12–14]. According to Rostamani et al. [15], this assumption may be realistic because the relative velocity decreases as the particle size decreases. This leads to a mixture that may be considered as a conventional single-phase fluid. Correlations for Nusselt number and friction factor of single-phase fluids are applicable, when effective physical properties of the nanofluid are known. A challenge is the provision of correct physical properties of nanofluids, as the available literature contains inconsistencies which are reported by [4, 14, 16–18], e.g. due to particle sedimentation, particle clustering and the unknown influence of additives and surfactants. The majority of numerical studies use the single-phase approach and report acceptable results for heat transfer and flow behaviour as stated by Kamyar et al. [19]. Other

studies concluded that a two-phase model is more accurate [19–22].

Using numerical simulation, Lotfi et al. [21] applied the two-phase Eulerian, mixture and single-phase model for laminar and turbulent flow. A comparison of calculated results and experimental values showed that the mixture model is more precise than the single-phase and two-phase Eulerian model, as both underestimated the Nusselt number.

For low particle concentrations ($\phi = 1\%$), Bianco et al. [22] found only small differences of results from simulations using two-phase mixture and single-phase model. At higher concentrations, significant deviations were observed and the two-phase mixture model delivered more accurate results. However, it was also mentioned that the accuracy of both models could be improved by more precise nanofluid physical properties.

Namburu et al. [23] investigated turbulent flow and heat transfer of three different nanofluids (CuO, Al_2O_3, SiO_2) in an ethylene glycol water mixture flowing through a circular tube under constant heat flux boundary condition. A single-phase approach was used with temperature dependent physical properties. The computed Nusselt numbers for nanofluids agreed well with a single-phase correlation. Small particle diameter nanofluids result in higher Nusselt numbers with CuO nanoparticles exhibiting the highest heat transfer enhancement.

Akbari et al. [24] studied the results of a single-phase model and three different two phase models (volume of fluid, mixture, Eulerian) for turbulent flow. They concluded that the single-phase model exhibited more accurate results than the tested two-phase models. Furthermore, single-phase models are simpler to implement and require less computer resources and central processing unit (CPU) time.

At this moment there is no consensus whether the single-phase approach is sufficient accurate to describe heat transfer. Therefore, the first objective of this work is to evaluate the single-phase approach by calculating Nusselt numbers and friction factors with a single-phase model and to compare the results with data from literature.

The viscosity of nanofluids rises with increasing particle concentration [4], and therefore also the pumping power. However, the heat transfer of nanofluids is generally superior to conventional single-phase fluids. This leads to the second objective of this study, which investigates whether the use of nanofluids can reduce the pumping power compared to a conventional fluid for equal heat flow rate.

MATHEMATICAL MODELLING

Tube heat exchanger

The numerical simulation in this work is based on the experimental set up and boundary conditions of Vajjha et al. [25], as shown in Figure 1. The experimental results will be used to evaluate the data from the numerical simulation. A steady, forced turbulent convection flow with Reynolds numbers ranging between $6000 \leq Re = (u_m \ d)/v \leq 12000$ and a constant heat flux is therefore considered. The fluid enters the tube with a fully developed velocity profile and a constant inlet temperature.

An ethylene glycol (EG) and water (W) mixture is used as base fluid (60:40 EG/W mass ratio) with 20 nm mean diameter SiO_2 nanoparticles dispersed in it. The particle volume concentrations ranges from 2% to 10%. For the numerical simulation, the physical properties of the nanofluid are assumed to be constant. The properties are taken at a temperature of 320 K. At this temperature the values of all quantities (thermal conductivity, viscosity and heat capacity) are available in literature. According to the experiment of Namburu et al. [26], the nanofluid exhibits a Newtonian behaviour for the studied temperature.

In this work, the behaviour of the nanofluid is modelled with the single-phase approach. It is assumed that flow and thermal fields are rotation-symmetric with respect to the pipe symmetry axis (two-dimensional simulation) and that base- and nanofluid are incompressible. Gravitational effects are neglected.

6

Governing equations

Within the numerical simulation, the Reynolds averaged continuity, momentum, and energy equation (Eqs. 1 to 3) for a Newtonian and Fourier fluid are solved.

$$\frac{\partial \overline{u}_i}{\partial x_i} = 0 \tag{1}$$

$$\frac{D\overline{u}_i}{Dt} = -\frac{\partial}{\partial x_i}\left(\frac{\overline{p}}{\rho} + \frac{2}{3}k\right) + \frac{\partial}{\partial x_j}\left[(\nu + \nu_t)\left(\frac{\partial \overline{u}_i}{\partial x_j} + \frac{\partial \overline{u}_j}{\partial x_i}\right)\right] \tag{2}$$

$$\frac{D\overline{T}}{Dt} = \frac{\partial}{\partial x_i}\left[\left(\frac{\nu}{Pr} + \frac{\nu_t}{Pr_t}\right)\frac{\partial \overline{T}}{\partial x_i}\right] \tag{3}$$

It was stated before that a steady state flow is considered. However, an unsteady solver was used due to convergence issues. Hence, the governing equations include the temporal derivative.

Turbulence modelling

For closure of the governing equations, the eddy viscosity ν_t and the turbulent kinetic energy k is calculated by the two-equation k-ω-SST-model [27], capable to resolve the viscous sublayer close to the wall (Low-Reynolds turbulence model). For this, the transport equations for the turbulent kinetic energy k (Eq. 4) and the specific dissipation rate ω (Eq. 5) have to be solved. Equation (6) is a blending function to calculate the model coefficients β, γ, σ_k and σ_ω, denoted with φ, by using the model coefficients of the original k-ω-model, denoted as φ_1, and the model coefficients of the transformed k-ε-model, denoted as φ_2. The eddy viscosity is calculated according to Eq. (7) using the model parameter a_1.

Model parameters used for this study are: $\sigma_{k1} = 0.85034$, $\sigma_{k2} = 1$, $\sigma_{\omega 1} = 0.5$, $\sigma_{\omega 2} = 0.85616$, $\beta_1 = 0.075$, $\beta_2 = 0.0828$, $\gamma_1 = 0.5532$, $\gamma_2 = 0.4403$, $\beta^* = 0.09$ and $a_1 = 0.31$. Further information about this turbulence model is available in the publication of Menter [27].

$$\frac{Dk}{Dt} = \frac{1}{\rho}\tau_{ij}\frac{\partial \overline{u}_i}{\partial x_j} - \beta^*\omega k + \frac{\partial}{\partial x_j}\left[(v + \sigma_k v_t)\frac{\partial k}{\partial x_j}\right] \tag{4}$$

$$\frac{D\omega}{Dt} = \frac{\gamma}{v_t}\frac{1}{\rho}\tau_{ij}\frac{\partial \overline{u}_i}{\partial x_j} - \beta\omega^2 + \frac{\partial}{\partial x_j}\left[(v + \sigma_\omega v_t)\frac{\partial \omega}{\partial x_j}\right] + 2(1 - F_1)\sigma_{\omega 2}\frac{1}{\omega}\frac{\partial k}{\partial x_j}\frac{\partial \omega}{\partial x_j} \tag{5}$$

$$\varphi = F_1\varphi_1 + (1 - F_1)\varphi_2 \tag{6}$$

$$v_t = \frac{a_1 k}{\max(a_1\omega; \Omega F_2)} \tag{7}$$

The turbulent Prandtl number Pr_t is necessary to close the system of equations for heat transfer when RANS turbulence models are used. In reality, the turbulent Prandtl number is a function of the distance to the wall [28–30]. However, a literature review in this field, especially the publication of Kays [28], suggested a constant turbulent Prandtl number of $Pr_t = 0.85$, which is applied in this work.

Numerical method

The computational fluid dynamics code OpenFOAM (Open source Field Operation And Manipulation) [31] version 2.3 is used for this study. OpenFOAM is based on the finite volume approach. The time derivatives are discretised with implicit Euler (first order) and the convective terms with Gauss upwind (first order).

The equation system to calculate the pressure field is solved by a PCG (Preconditioned Conjugate Gradient) solver with the DIC (Diagonal Incomplete-Cholesky) preconditioner for symmetric matrices. A smooth solver with Gauss-Seidel smoother was used for the velocity u, temperature T, turbulent kinetic energy k and specific turbulence dissipation rate ω.

Residuals for the pressure were in the range of 6.6×10^{-5} to 9.4×10^{-5}, with lower residuals for lower Reynolds numbers. Residuals for k, ω, T and u_x were all below 10^{-7}. The velocity in y- and z-direction exhibited higher residuals, 10^{-2} and 10^{-3}, respectively. However, the velocities in y- and z-direction were in order of 10^{-22} and 10^{-8}, respectively,

for a mean velocity in x-direction in order of 1.

Grid

A two-dimensional, rotation-symmetric geometry with only one cell in circumferential direction is considered for the tube heat exchanger in the numerical simulation. Note that in Figure 2 the cell number in z-direction is reduced to 33 to visualize the grid topology. To resolve the viscous sublayer the non-dimensional wall distance is set to $y^+ = 0.5$. For all cases the cell number in x-direction was 150. Depending on the Reynolds number, the number of cells in z-direction was varying between 66 and 84.

Boundary conditions

At the tube heat exchanger inlet, uniform temperature T_{in}, fully developed profiles for velocity u_i, turbulent kinetic energy k and specific dissipation rate ω from previous calculations have been specified. Fully developed profiles are assumed for the outlet, and therefore zero normal gradients are set for all variables except pressure. Symmetry boundary conditions are chosen for the symmetry surfaces. No-slip, constant heat flux, zero normal gradient for the pressure and zero turbulent kinetic energy $k = 0$ boundary conditions are applied to the wall. Furthermore, continues wall functions for eddy viscosity ν_t using Spaldings single formula for the wall [32] and specific turbulence dissipation rate ω proposed by Menter and Esch [33] are applied.

Physical properties of nanofluids

The following correlations have been used to calculate the physical properties of the investigated nanofluid for the numerical simulation.

Vajjha and Das [34] analysed experimental data of nanofluids with SiO_2, Al_2O_3, and CuO particles and proposed a new correlation for the dynamic viscosity in a non-dimensional form,

valid for all three nanofluids, which was cited by Vajjha and Das [35].

$$\frac{\mu_{nf}}{\mu_{bf}} = A_1 \exp(A_2 \phi) \tag{8}$$

For 20 nm SiO₂ particles and particle volume concentrations of $0\% < \phi < 10\%$ they give the parameters $A_1 = 1.092$ and $A_2 = 5.954$.

Sahoo et al. [36] experimentally studied the thermal conductivity of SiO₂ nanoparticles dispersed in an ethylene glycol and water mixture. They proposed a new correlation based on the model of Koo and Kleinstreuer [37] and adapted it for non-metallic SiO₂ nanoparticles.

$$\lambda_{nf} = \frac{\lambda_p + 2\lambda_{bf} - 2(\lambda_{bf} - \lambda_p)\phi}{\lambda_p + 2\lambda_{bf} + (\lambda_{bf} - \lambda_p)\phi} \lambda_{bf} + 5 \cdot 10^4 \beta \ \phi \ \rho_{bf} \ c_{p,bf} \sqrt{\frac{k_B T}{\rho_p \ d_p}} f(T, \phi) \tag{9}$$

$$\beta = 1.9526(100\phi)^{-1.4594} \tag{10}$$

$$f(T, \phi) = \left(\frac{2.8217}{10^2}\phi + \frac{3.917}{10^3}\right)\left(\frac{T}{T_0}\right) + \left(-\frac{3.0669}{10^2}\phi - \frac{3.91123}{10^3}\right) \tag{11}$$

Reference temperature is $T_0 = 273$ K and the Boltzmann constant is $k_B = 1.381 \cdot 10^{-23}$ J/K. Equations (9) to (11) are valid for $1\% \leq \phi \leq 10\%$ and $298\,\text{K} < T < 365\,\text{K}$.

Vajjha and Das [38] measured the specific heat capacity of three nanofluids and developed a new correlation which can be used for different base fluids. However, this correlation was slightly modified by Vajjha and Das [35] in 2012, so that the latest version will be used.

$$\frac{c_{p,nf}}{c_{p,bf}} = \frac{A\frac{T}{T_0} + B\frac{c_{p,p}}{c_{p,bf}}}{C + \phi} \tag{12}$$

The reference temperature is $T_0 = 273$ K. The empirical parameters for SiO₂ nanoparticles are $A = 0.48294$, $B = 1.1937$ and $C = 0.8021$. Equation (12) for SiO₂ particles is valid for $0\% \leq \phi \leq 10\%$ and $315\,\text{K} < T < 363\,\text{K}$.

The properties of silicon dioxide (fused silica) are given by Incropera et al. [39, p. 934] for

300 K: $\rho = 2220$ kg/m³, $c_p = 745$ J/(kg K), $\lambda = 1.4$ W/(m K).

Vajjha and Das [35] fitted functions to physical properties of the base fluid (60% ethylene glycol and 40% water mass ratio) provided by the ASHRAE Handbook [40].

$$\mu_{bf} \text{ [Pa s]} = 0.555 \cdot 10^{-6} \exp(2664/T) \qquad (13)$$

$$\lambda_{bf} \text{ [W/(m K)]} = -3 \cdot 10^{-6} T^2 + 0.0025T - 0.1057 \qquad (14)$$

$$c_{p,bf} \text{ [J/(kg K)]} = 4.2483T + 1882.4 \qquad (15)$$

Equations (13) to (15) are valid within the temperature range of $293 \text{ K} \le T \le 363 \text{ K}$ and the coefficient of determination is at least 0.97.

Data analysis

To estimate the accuracy of the numerical simulation, a comparison of own numerical results with correlations for single-phase fluids from literature is carried out (Figures 3 and 5). Further comparisons with correlations for nanofluids enables conclusion, whether the single-phase approach is suitable to describe momentum and heat transfer of nanofluids (Figures 4 and 6). Below the used correlations are given.

To calculate the friction factor the density is necessary. Vajjha et al. [41] measured the density of ethylene glycol/water containing different nanoparticles (aluminium oxide, antimony tin oxide, and zinc oxide) and compared the results with the theoretical equation by Pak and Cho [12]. According to Vajjha and Das [35], it is also applicable for CuO and SiO_2 particles.

$$\rho_{nf} = \rho_p \phi + \rho_{bf}(1 - \phi) \qquad (16)$$

Equation (17) is a curve-fitted equation by Vajjha and Das [35] for a 60% ethylene glycol and 40% water mass ratio mixture.

$$\rho_{bf} \text{ [kg/m}^3] = -0.0024T^2 + 0.963T + 1009.8 \qquad (17)$$

11

The friction factor is compared to Eq. (18), a relation for flows in smooth tubes by Blasius and cited by Oertel et al. [42, p. 150], which is valid for the studied range of Reynolds numbers.

$$f = \frac{0.3164}{Re^{0.25}} \tag{18}$$

Vajjha et al. [25] proposed Eq. (19) valid for SiO_2 nanofluids with $4000 < Re < 16000$ and $0\% \leq \phi \leq 6\%$.

$$f_{nf} = \frac{0.3164}{Re_{nf}^{0.25}} \left(\frac{\rho_{nf}}{\rho_{bf}}\right)^{0.797} \left(\frac{\mu_{nf}}{\mu_{bf}}\right)^{0.108} \tag{19}$$

Gnielinski [43] proposed Eq. (20) to predict the Nusselt number of turbulent flow in tubes with constant heat flux for single-phase fluids. It is valid for $2300 \leq Re \leq 10^6$, $0.5 \leq Pr \leq 2000$ and $0 \leq d/L \leq 1$. Equation (18) is used as friction factor f in Eq. (20). Gnielinski [43] stated that Eq. (20) is accurate within $\pm20\%$ and Bejan and Kraus [44, p. 425] note that it is accurate within $\pm10\%$.

$$Nu = \frac{\frac{f}{8}(Re - 1000)Pr}{1 + 12.7\sqrt{\frac{f}{8}}\left(Pr^{\frac{2}{3}} - 1\right)}\left[1 + \left(\frac{d}{L}\right)^{\frac{2}{3}}\right] \tag{20}$$

For comparison of the pumping power nanofluid/base fluid an additional Nusselt number correlation, Eq. (21), for single-phase fluids by Gnielinski [43] was used.

$$Nu = 0.012(Re^{0.87} - 280)Pr^{0.4} \tag{21}$$

Equation (21) is valid for $3000 \leq Re \leq 10^6$ and $1.5 \leq Pr \leq 500$. According to Gnielinski [43], Eq. (21) has the capability to calculate Nusselt numbers with an accuracy of $\pm20\%$.

Vajjha et al. [25] proposed Eq. (22) for the Nusselt number of SiO_2 nanofluids with $3000 < Re < 16000$ and $0\% < \phi < 10\%$. It has a maximum deviation of $\pm10\%$ and an average deviation of 2% when compared with the experimental data points.

$$Nu_{nf} = 0.065\left(Re_{nf}^{0.65} - 60.22\right)\left(1 + 0.0169\phi^{0.15}\right)Pr_{nf}^{0.542} \tag{22}$$

RESULTS AND DISCUSSION

Friction factor and Nusselt number

Figure 3 displays the comparison of friction factors for the numerically obtained results with values according to the equation of Blasius (Eq. 18). A maximum deviation of 3.2% and a mean deviation of 0.5% indicate excellent agreement. As expected, the friction factor is independent from the studied Prandtl number (nanofluid concentration), because the solution of continuity and momentum equation does not require the energy equation. Therefore, only four data points with the studied Reynolds numbers are presented.

In comparison to the correlation of Vajjha et al. [25] (Eq. 19), the values of this work underestimate the friction factor. Figure 4 presents the friction factors of the base fluid, nanofluid and the numerical simulation with physical properties evaluated at 320 K. The nanofluid friction factors deviate from the single-phase friction factors and the deviation is increasing with higher particle volume concentrations. This could be explained by a relative movement between fluid and nanoparticles which may lead to an additional momentum transport and an increase in friction factor. On the other hand, Heyhat et al. [45] concluded in their experimental turbulent heat transfer study of Al_2O_3–water nanofluids, that pressure drop can be predicted with the help of the traditional correlations and models, if the effective nanofluid properties are used. However, this might not be the case for the studied SiO_2, ethylene glycol and water mixture nanofluid, as there is no general theory for effective nanofluid properties. Hence, various nanofluids might behave differently.

Figure 5 presents the comparison of the Nusselt numbers by Gnielinski, Eq. (20), and computed Nusselt numbers. The computed values exhibit an average deviation of -4.5% and a maximum deviation of -9.5%, which are in the limits proposed by Gnielinski [43]. However, the deviation increases with increasing Reynolds number and the simulation starts to

13

underestimate the Nusselt number. Furthermore, higher Prandtl numbers (higher concentrations) usually result in higher deviations.

Figure 6 shows a comparison of the Nusselt number correlation by Vajjha et al. [25], Eq. (22), and computed Nusselt numbers for $\phi \geq 2\%$. It can be observed that the computed values underestimate the Nusselt numbers for lower Reynolds numbers and start to approach the predicted Nusselt number as the Reynolds number increases. Again, higher Prandtl numbers (higher concentrations) usually lead to higher deviations. This results in a mean deviation of -5.6% and a maximum deviation of -11.9%, which are higher than stated for Eq. (22). However, these deviations are not unusual for Nusselt number predictions.

Figure 7 displays the computed Nusselt numbers of base- and nanofluid for the studied Reynolds numbers with varying particle volume concentration. The Nusselt number is increasing with rising Reynolds number, due to the diminishing thickness of the viscous sublayer and the increasing turbulent transport of thermal energy. All studied nanofluid concentrations exhibit higher Nusselt numbers in comparison to those of the base fluid. An increase in Nusselt number occurs with rise in particle concentration. This is mainly caused by the increase in thermal conductivity of the nanofluid. Within the investigated parameter domain, the maximum change in Nusselt number appears at $Re = 12000$ and $\phi = 10\%$ and amounts to 13.2%. It has to be mentioned that this lays within the accuracy of the used correlations. The positive slope in Figure 7 results from the increase in Prandtl number with rising particle concentration, as shown in Figure 8.

Comparison of pumping power

Nanofluids exhibit higher viscosities than the base fluid and therefore cause a higher pressure drop at a constant Reynolds number and tube diameter. However, nanofluids feature superior Nusselt numbers (Figure 7). Hence, an equal heat flow rate can be obtained at a lower Reynolds number. In the following, a comparison of pumping power for nanofluid and base

14

fluid at equal heat flow rate ($\dot{Q}_{bf} = \dot{Q}_{nf}$) is presented. The pumping power of the flow in a pipe can be expressed as

$$P = \dot{V}\Delta p = \frac{\pi}{8} L \frac{1}{d^2} f \frac{1}{\rho^2} \mu^3 Re^3 \tag{23}$$

The heat flow rate is

$$\dot{Q} = \alpha A \Delta T \tag{24}$$

The convective heat transfer coefficient α is set constant as well as the geometry to establish comparable conditions for the pumping power and heat transfer of base- and nanofluid. The convective heat transfer coefficient α is calculated by

$$\alpha = \frac{Nu\ \lambda}{d} \tag{25}$$

An equation for the nanofluid Nusselt number can be formed when the expression of Eq. (25) is set equal for the base- and nanofluid.

$$Nu_{nf} = Nu_{bf} \frac{\lambda_{bf}}{\lambda_{nf}} \tag{26}$$

The pumping power ratio for the same heat flow rate of base and nanofluid is

$$\frac{P_{nf}}{P_{bf}} = \frac{f_{nf}}{f_{bf}} \left(\frac{\rho_{bf}}{\rho_{nf}}\right)^2 \left(\frac{\mu_{nf}}{\mu_{bf}}\right)^3 \left(\frac{Re_{nf}}{Re_{bf}}\right)^3 \tag{27}$$

The parameters of Eq. (27) are calculated in the following sequence: (1) For a chosen base fluid Reynolds number Re_{bf} the Nusselt number Nu_{bf} is taken from numerical results or calculated with conventional correlations (Eqs. 20 and 21). (2) Equation (26) leads to the Nusselt number of the nanofluid Nu_{nf}. (3) Afterwards it is possible to calculate the nanofluid Reynolds number Re_{nf} by using the nanofluid Nusselt number Nu_{nf} and the simulation results or Eq. (22). (4) The power ratio results from Eq. (27) using the Reynolds numbers Re_{bf}

and Re_{nf} as well as the ratios of density and viscosity.

Figures 9 and 10 display the pumping power ratio according to Eq. (27) for the computed results and two theoretical cases with physical properties evaluated at 320 K, exemplary for $Re_{bf} = 6000$ and 8000. Table 1 shows the physical property ratios of Eq. (27). The line definitions of Figures 9 and 10 are given in the following:

- Solid line: Nu_{nf} (Eq. 26), all other parameters of Eq. (27) are calculated with interpolated equations of the numerical results

- Dashed line: Nu_{bf} (Eq. 20), Nu_{nf} (Eq. 26), Re_{nf} (Eq. 22), f_{bf} (Eq. 18), f_{nf} (Eq. 19)

- Dotted line: Nu_{bf} (Eq. 21), other parameters are equal to the definitions of the dashed line

Note that ratios were only calculated till a particle volume concentration of $\phi = 6\%$, because this is the maximum valid concentration of Eq. (19). Furthermore, the additional term $1 + (d/L)^{2/3}$ of Eq. (20) was not considered for this comparison, due to fully developed flow. In addition, no pumping power ratio was calculated for the dotted case in Figure 9 at $\phi = 6\%$, because the necessary nanofluid Reynolds number was below $Re = 4000$ and Eq. (19) is only valid for $Re > 4000$.

Figures 9 and 10 indicate the possibility of a local pumping power ratio minimum for lower particle concentrations and Reynolds numbers. The pumping power ratio is generally increasing for higher particle concentrations and Reynolds numbers. Values for pumping power ratio of the computed results (solid line) only differ marginally from each other due to slight changes in f_{nf}/f_{bf} and a nearly constant ratio of Re_{nf}/Re_{bf}. The latter is caused by the almost constant rise of Nusselt number (Figure 7). For all used Nusselt data and correlations, respectively, it becomes apparent that the superior heat transfer performance of higher nanoparticle concentrations is not sufficient to overcome the viscosity increase.

16

In both figures, high deviations occur between the plotted curves. This results from the non-linear influence of Re_{nf}/Re_{bf} in Eq. (27). Furthermore, even the theoretical cases (dashed and dotted lines) differ considerably and show the significance of the base fluid Nusselt number Nu_{bf} on the pumping power ratio. Similar comparisons were also performed for $Re_{bf} = 10000$ and $Re_{bf} = 12000$, which indicate the same trend described before.

The results do not allow a statement whether the pumping power can be reduced with nanofluids nor how high the savings may be. However, it should be noted that the comparison was performed with physical properties evaluated at 320 K. Vajjha and Das [35] carried out a comparison similar to the dotted case for varying temperature. They indicated that low concentration nanofluids exhibit pumping power savings compared to the base fluid for low temperatures. A superior performance compared to the base fluid for lower temperatures supports the area of application for ethylene glycol and water mixtures, as it is a commonly used fluid in cold regions.

CONCLUSIONS

The validity of the single- and two-phase approach for nanofluid modelling is not fully analysed, yet. This study showed that the single-phase approach cannot predict the higher nanofluid friction factors observed by Vajjha et al. [25]. However, Nusselt number predictions were quite accurate with mean deviations in the range of -5%. It should be analysed if the higher nanofluid friction factor can be reproduced with a two-phase model.

It cannot be stated that the nanofluid pumping power is less than the base fluid pumping power for equal heat transfer rate, due to the highly differing ratios in Figures 9 and 10. The results indicate that the nanofluid requires more pumping power than the base fluid for high particle concentrations and Reynolds numbers.

Low particle volume concentrations should be especially considered in future studies, as they provide an increase of heat transfer rate and a possible reduction of pumping power. This

17

was also stated by Wu and Zhao [4].

Additional nanoparticle materials should be studied in future. Das et al. [46] state that oxide nanoparticle-based nanofluids are less promising in the enhancement of thermal conductivity of fluids than metallic nanoparticles, which seem to enhance the thermal conductivity anomalously. However, highly thermal conductive materials are not always the best candidates for the suspension in improving the thermal transport property of fluids [47–49]. This shows, that there are still many questions unanswered concerning the effects of nanoparticles on physical properties and heat transfer, which should be primarily addressed in future studies.

NOMENCLATURE

A	Area, m^2
c_p	Specific heat capacity, $J.kg^{-1}.K^{-1}$
d	Diameter, m
f	Friction factor, dimensionless
F_1	Variable for the Menter [27] turbulence model, dimensionless
F_2	Variable for the Menter [27] turbulence model, dimensionless
k	Turbulent kinetic energy, $m^2.s^{-2}$
k_B	Boltzmann constant, $J.K^{-1}$
L	Length, m
Nu	Nusselt number, dimensionless
p	Pressure, Pa
$\overline{p}$	Time-averaged pressure, Pa
P	Pumping power, W
Pr	Prandtl number, dimensionless
Pr_t	Turbulent Prandtl number, dimensionless
$\dot{q}$	Heat flux, $W.m^{-2}$
$\dot{Q}$	Heat flow rate, W
Re	Reynolds number, dimensionless
t	Time, s
T	Temperature, K
T_0	Reference temperature, K
$\overline{T}$	Time-averaged temperature, K

18

u	Velocity, m.s^{-1}
$\overline{u}$	Time-averaged velocity, m.s^{-1}
$\dot{V}$	Volumetric flow rate, m^3.s^{-1}
x	Coordinate, m
y	Coordinate, m
y^+	Non-dimensional wall distance, dimensionless
z	Coordinate, m

Greek symbols

α	Convective heat transfer coefficient, W.m^{-2}.K^{-1}
Δ	Difference, dimensionless
ε	Turbulence dissipation rate, J.kg^{-1}.s^{-1}
λ	Thermal conductivity, W.m^{-1}.K^{-1}
μ	Dynamic viscosity, Pa.s
ν	Kinematic viscosity, m^2.s^{-1}
ν_t	Eddy viscosity, m^2.s^{-1}
ω	Specific dissipation rate, s^{-1}
Ω	Vorticity, s^{-1}
ϕ	Nanoparticle volume concentration, dimensionless
ρ	Density, kg.m^{-3}
τ	Total stress tensor, N.m^{-2}

Subscripts

bf	Base fluid
i,j	Index notation
in	Inlet
m	Mean
nf	Nanofluid
out	Outlet
p	Particle
x	Coordinate

REFERENCES

[1]   Choi, S. U. S., and Eastman, J. A., Enhancing thermal conductivity of fluids with nanoparticles, ANL/MSD/CP-84938, October 1995.

[2]   Maïga, S. E. B., Palm, S. J., Nguyen, C. T., Roy, G., and Galanis, N., Heat transfer enhancement by using nanofluids in forced convection flows, *International Journal of Heat and Fluid Flow*, vol. 26, no. 4, pp. 530–546, 2005.

[3]   Chandrasekar, M., and Suresh, S., A Review on the Mechanisms of Heat Transport in Nanofluids, *Heat Transfer Engineering*, vol. 30, no. 14, pp. 1136–1150, 2009.

[4]   Wu, J. M., and Zhao, J., A review of nanofluid heat transfer and critical heat flux enhancement-Research gap to engineering application, *Progress in Nuclear Energy*, vol. 66, pp. 13–24, 2013.

[5]   Huminic, G., and Huminic, A., Application of nanofluids in heat exchangers: a review, *Renewable and Sustainable Energy Reviews*, vol. 16, no. 8, pp. 5625–5638, 2012.

[6]   Kulkarni, D. P., Das, D. K., and Vajjha, R. S., Application of nanofluids in heating buildings and reducing pollution, *Applied Energy*, vol. 86, no. 12, pp. 2566–2573, 2009.

[7]   Yu, W., France, D. M., Routbort, J. L., and Choi, S. U. S., Review and Comparison of Nanofluid Thermal Conductivity and Heat Transfer Enhancements, *Heat Transfer Engineering*, vol. 29, no. 5, pp. 432–460, 2008.

[8]   De Risi, A., Milanese, M., Colangelo, G., and Laforgia, D., High efficiency nanofluid cooling system for wind turbines, *Thermal Science*, vol. 18, no. 2, pp. 543–554, 2014.

[9]   Otanicar, T. P., Phelan, P. E., Prasher, R. S., Rosengarten, G., and Taylor, R. A., Nanofluid-based direct absorption solar collector, *Journal of renewable and sustainable energy*, vol. 2, no. 3, p. 33102, 2010.

20

[10] Colangelo, G., Favale, E., De Risi, A., and Laforgia, D., A new solution for reduced sedimentation flat panel solar thermal collector using nanofluids, *Applied Energy*, vol. 111, pp. 80–93, 2013.

[11] Colangelo, G., Favale, E., Miglietta, P., De Risi, A., Milanese, M., and Laforgia, D., Experimental test of an innovative high concentration nanofluid solar collector, *Applied Energy*, vol. 154, pp. 874–881, 2015.

[12] Pak, B. C., and Cho, Y. I., Hydrodynamic and heat transfer study of dispersed fluids with submicron metallic oxide particles, *Experimental Heat Transfer an International Journal*, vol. 11, no. 2, pp. 151–170, 1998.

[13] Xuan, Y., and Li, Q., Investigation on convective heat transfer and flow features of nanofluids, *Journal of Heat Transfer*, vol. 125, no. 1, pp. 151–155, 2003.

[14] Xuan, Y., and Li, Q., Heat transfer enhancement of nanofluids, *International Journal of Heat and Fluid Flow*, vol. 21, no. 1, pp. 58–64, 2000.

[15] Rostamani, M., Hosseinizadeh, S. F., Gorji, M., and Khodadadi, J. M., Numerical study of turbulent forced convection flow of nanofluids in a long horizontal duct considering variable properties, *International Communications in Heat and Mass Transfer*, vol. 37, no. 10, pp. 1426–1431, 2010.

[16] Lomascolo, M., Colangelo, G., Milanese, M., and Risi, A. de, Review of heat transfer in nanofluids, *Renewable and Sustainable Energy Reviews*, vol. 43, pp. 1182–1198, 2015.

[17] Aybar, H. Ş., Sharifpur, M., Azizian, M. R., Mehrabi, M., and Meyer, J. P., A Review of Thermal Conductivity Models for Nanofluids, *Heat Transfer Engineering*, vol. 36, no. 13, pp. 1085–1110, 2015.

[18] Wen, D., Lin, G., Vafaei, S., and Zhang, K., Review of nanofluids for heat transfer

applications, *Particuology*, vol. 7, no. 2, pp. 141–150, 2009.

[19] Kamyar, A., Saidur, R., and Hasanuzzaman, M., Application of computational fluid dynamics (CFD) for nanofluids, *International Journal of Heat and Mass Transfer*, vol. 55, no. 15, pp. 4104–4115, 2012.

[20] Haghshenas Fard, M., Esfahany, M. N., and Talaie, Numerical study of convective heat transfer of nanofluids in a circular tube two-phase model versus single-phase model, *International Communications in Heat and Mass Transfer*, vol. 37, no. 1, pp. 91–97, 2010.

[21] Lotfi, R., Saboohi, Y., and Am Rashidi, Numerical study of forced convective heat transfer of nanofluids: comparison of different approaches, *International Communications in Heat and Mass Transfer*, vol. 37, no. 1, pp. 74–78, 2010.

[22] Bianco, V., Manca, O., and Nardini, S., Numerical investigation on nanofluids turbulent convection heat transfer inside a circular tube, *International Journal of Thermal Sciences*, vol. 50, no. 3, pp. 341–349, 2011.

[23] Namburu, P. K., Das, D. K., Tanguturi, K. M., and Vajjha, R. S., Numerical study of turbulent flow and heat transfer characteristics of nanofluids considering variable properties, *International Journal of Thermal Sciences*, vol. 48, no. 2, pp. 290–302, 2009.

[24] Akbari, M., Galanis, N., and Behzadmehr, A., Comparative assessment of single and two-phase models for numerical studies of nanofluid turbulent forced convection, *International Journal of Heat and Fluid Flow*, vol. 37, pp. 136–146, 2012.

[25] Vajjha, R. S., Das, D. K., and Kulkarni, D. P., Development of new correlations for convective heat transfer and friction factor in turbulent regime for nanofluids, *International Journal of Heat and Mass Transfer*, vol. 53, no. 21, pp. 4607–4618, 2010.

[26] Namburu, P. K., Kulkarni, D. P., Dandekar, A., and Das, D. K., Experimental investigation of viscosity and specific heat of silicon dioxide nanofluids, *Micro & Nano Letters, IET*, vol. 2, no. 3, pp. 67–71, 2007.

[27] Menter, F. R., Two-equation eddy-viscosity turbulence models for engineering applications, *AIAA journal*, vol. 32, no. 8, pp. 1598–1605, 1994.

[28] Kays, W. M., Turbulent Prandtl number-Where are we?, *Journal of Heat Transfer*, vol. 116, no. 2, pp. 284–295, 1994.

[29] Abraham, J. P., Sparrow, E. M., and Tong, J. C., Heat transfer in all pipe flow regimes: laminar, transitional/intermittent, and turbulent, *International Journal of Heat and Mass Transfer*, vol. 52, no. 3, pp. 557–563, 2009.

[30] Srinivasan, C., and Papavassiliou, D. V., Prediction of the turbulent Prandtl number in wall flows with Lagrangian simulations, *Industrial & Engineering Chemistry Research*, vol. 50, no. 15, pp. 8881–8891, 2010.

[31] Weller, H. G., Tabor, G., Jasak, H., and Fureby, C., A tensorial approach to computational continuum mechanics using object-oriented techniques, *Computers in Physics*, vol. 12, no. 6, pp. 620–631, 1998.

[32] Spalding, D. B., A single formula for the "law of the wall", *Journal of Applied Mechanics*, vol. 28, no. 3, pp. 455–458, 1961.

[33] Menter, F.; Esch, T., Elements of industrial heat transfer predictions, *Proc. 16th Brazilian Conference of Mechanical Engineering (COBEM 2001)*, Uberlândia, Brazil, pp. 117–127, 2001.

[34] Vajjha, R. S., *Measurements of Thermophysical Properties of Nanofluids and Computation of Heat Transfer Characteristics*, University of Alaska Fairbanks, Fairbanks, 2008.

[35] Vajjha, R. S., and Das, D. K., A review and analysis on influence of temperature and concentration of nanofluids on thermophysical properties, heat transfer and pumping power, *International Journal of Heat and Mass Transfer*, vol. 55, no. 15, pp. 4063–4078, 2012.

[36] Sahoo, B. C., Das, D. K., Vajjha, R. S., and Satti, J. R., Measurement of the thermal conductivity of silicon dioxide nanofluid and development of correlations, *Journal of Nanotechnology in Engineering and Medicine*, vol. 3, no. 4, p. 41006, 2012.

[37] Koo, J., and Kleinstreuer, C., A new thermal conductivity model for nanofluids, *Journal of Nanoparticle Research*, vol. 6, no. 6, pp. 577–588, 2004.

[38] Vajjha, R. S., and Das, D. K., Specific heat measurement of three nanofluids and development of new correlations, *Journal of Heat Transfer*, vol. 131, no. 7, p. 71601, 2009.

[39] Incropera, F. P., Dewitt, D., Bergman, T. L., and Lavine, A. S., *Fundamentals of heat and mass transfer*, 6th ed., John Wiley & Sons, Hoboken, 2007.

[40] American Society of Heating, Refrigerating and Air-Conditioning Engineers, *ASHRAE Handbook - Fundamentals*, ASHRAE, Atlanta, 2005.

[41] Vajjha, R. S., Das, D. K., and Mahagaonkar, B. M., Density measurement of different nanofluids and their comparison with theory, *Petroleum Science and Technology*, vol. 27, no. 6, pp. 612–624, 2009.

[42] Oertel, H., Böhle, M., Ehrhard, P., Etling, D., Müller, U., Riedel, U., and Sreenivasan, K. R., *Prandtl-Führer durch die Strömungslehre: Grundlagen und Phänomene*, 13th ed., Springer Vieweg, Wiesbaden, 2012.

[43] Gnielinski, V., Neue Gleichungen für den Wärme-und den Stoffübergang in turbulent durchströmten Rohren und Kanälen, *Forschung im Ingenieurwesen A*, vol. 41, no. 1,

pp. 8–16, 1975.

[44] Bejan, A., and Kraus, A. D., *Heat transfer handbook*, 1ˢᵗ ed., John Wiley & Sons, Hoboken, 2003.

[45] Heyhat, M. M., Kowsary, F., Am Rashidi, Alem Varzane Esfehani, S., and Amrollahi, A., Experimental investigation of turbulent flow and convective heat transfer characteristics of alumina water nanofluids in fully developed flow regime, *International Communications in Heat and Mass Transfer*, vol. 39, no. 8, pp. 1272–1278, 2012.

[46] Das, S. K., Choi, S. U. S., and Patel, H. E., Heat Transfer in Nanofluids-A Review, *Heat Transfer Engineering*, vol. 27, no. 10, pp. 3–19, 2006.

[47] Gu, B., Hou, B., Lu, Z., Wang, Z., and Chen, S., Thermal conductivity of nanofluids containing high aspect ratio fillers, *International Journal of Heat and Mass Transfer*, vol. 64, pp. 108–114, 2013.

[48] Hong, K. S., Hong, T.-K., and Yang, H.-S., Thermal conductivity of Fe nanofluids depending on the cluster size of nanoparticles, *Applied Physics Letters*, vol. 88, no. 3, p. 31901, 2006.

[49] Zhu, H., Zhang, C., Liu, S., Tang, Y., and Yin, Y., Effects of nanoparticle clustering and alignment on thermal conductivities of Fe3O4 aqueous nanofluids, *Applied Physics Letters*, vol. 89, no. 2, p. 23123, 2006.

Table 1 Physical property ratios of the pumping power ratio

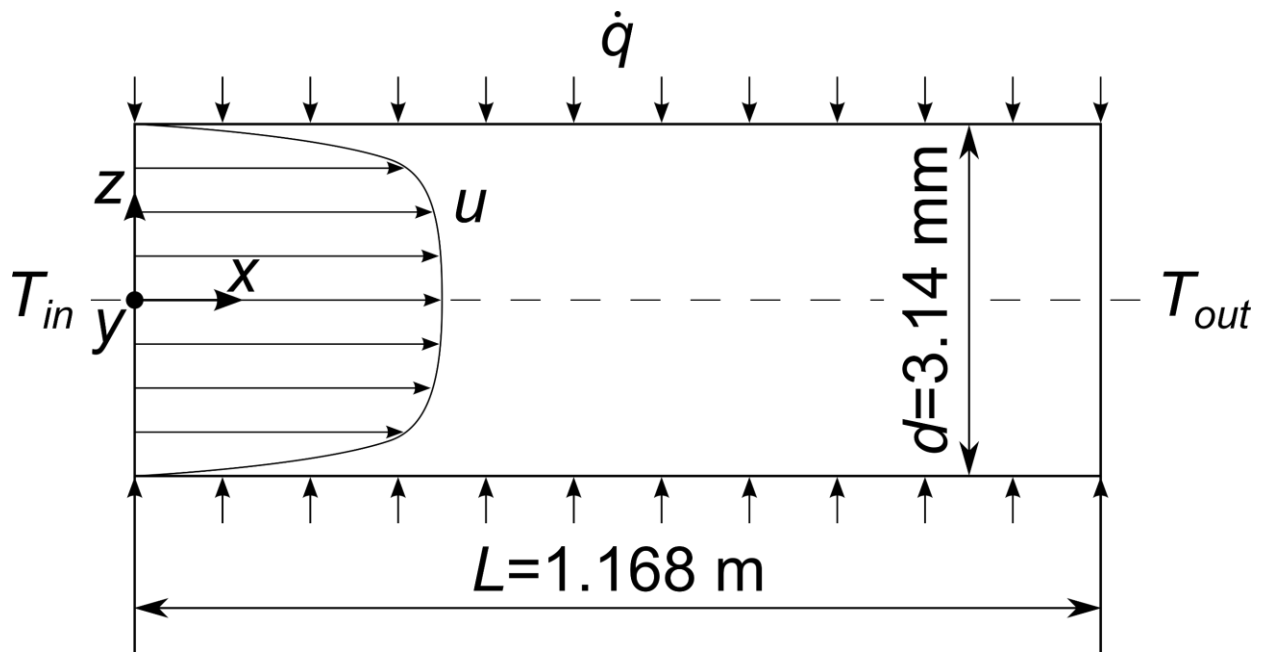|	$\phi = 2\%$	$\phi = 4\%$	$\phi = 6\%$
$\left(\dfrac{\rho_{bf}}{\rho_{nf}}\right)^2$	0.96	0.92	0.88
$\left(\dfrac{\mu_{nf}}{\mu_{bf}}\right)^3$	1.86	2.66	3.8

LIST OF FIGURE CAPTIONS

Figure 1 Schematic diagram of the tube heat exchanger and boundary conditions

Figure 2 Grid example with reduced cell number in z-direction
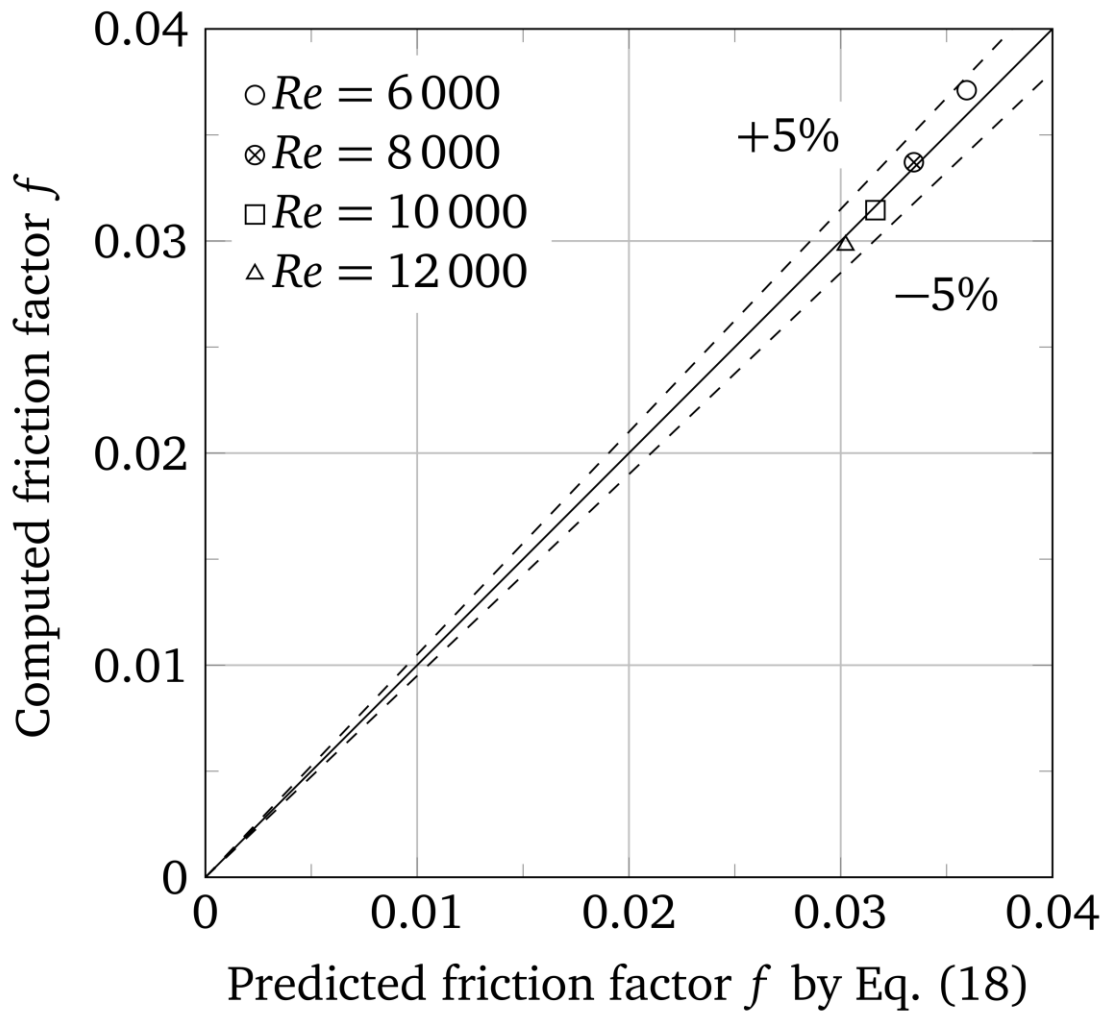
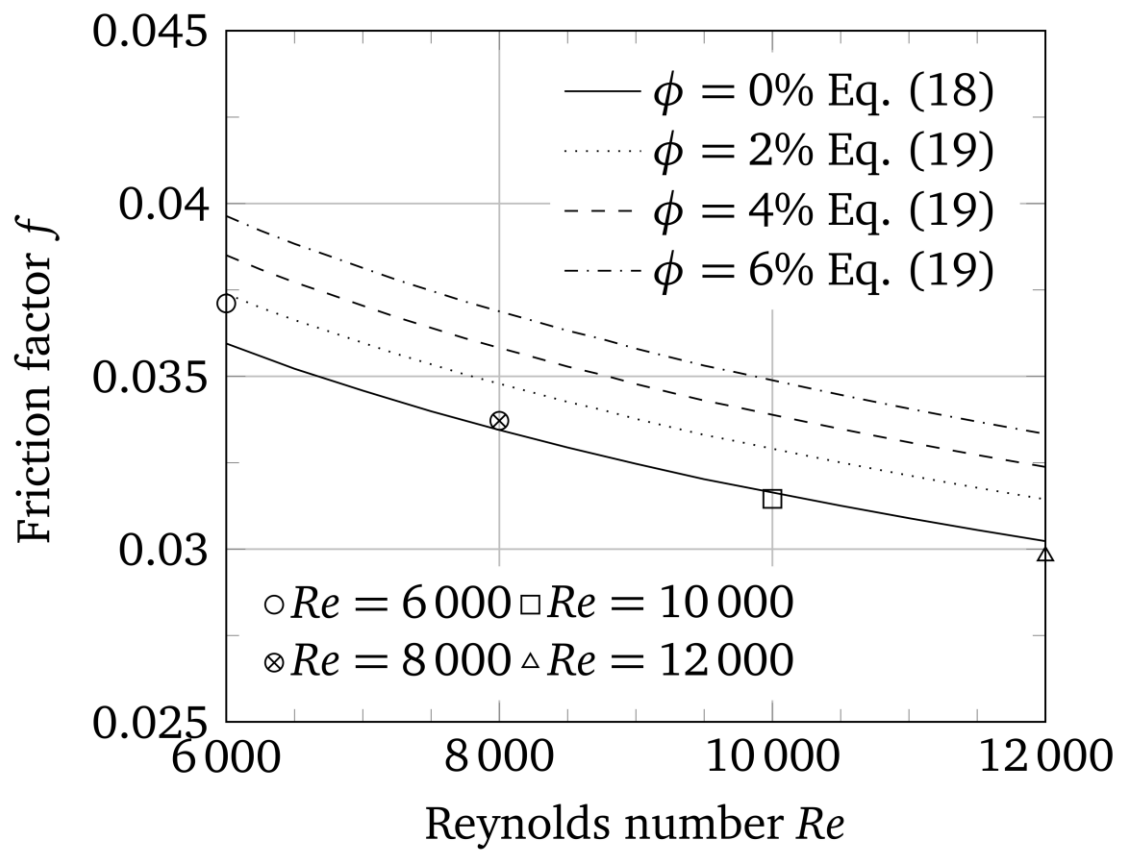Figure 3 Comparison of the friction factor by Blasius and computed values

Figure 4 Friction factor for base- and nanofluid (Eqs. 18 and 19) with varying Reynolds number in comparison with computed friction factors
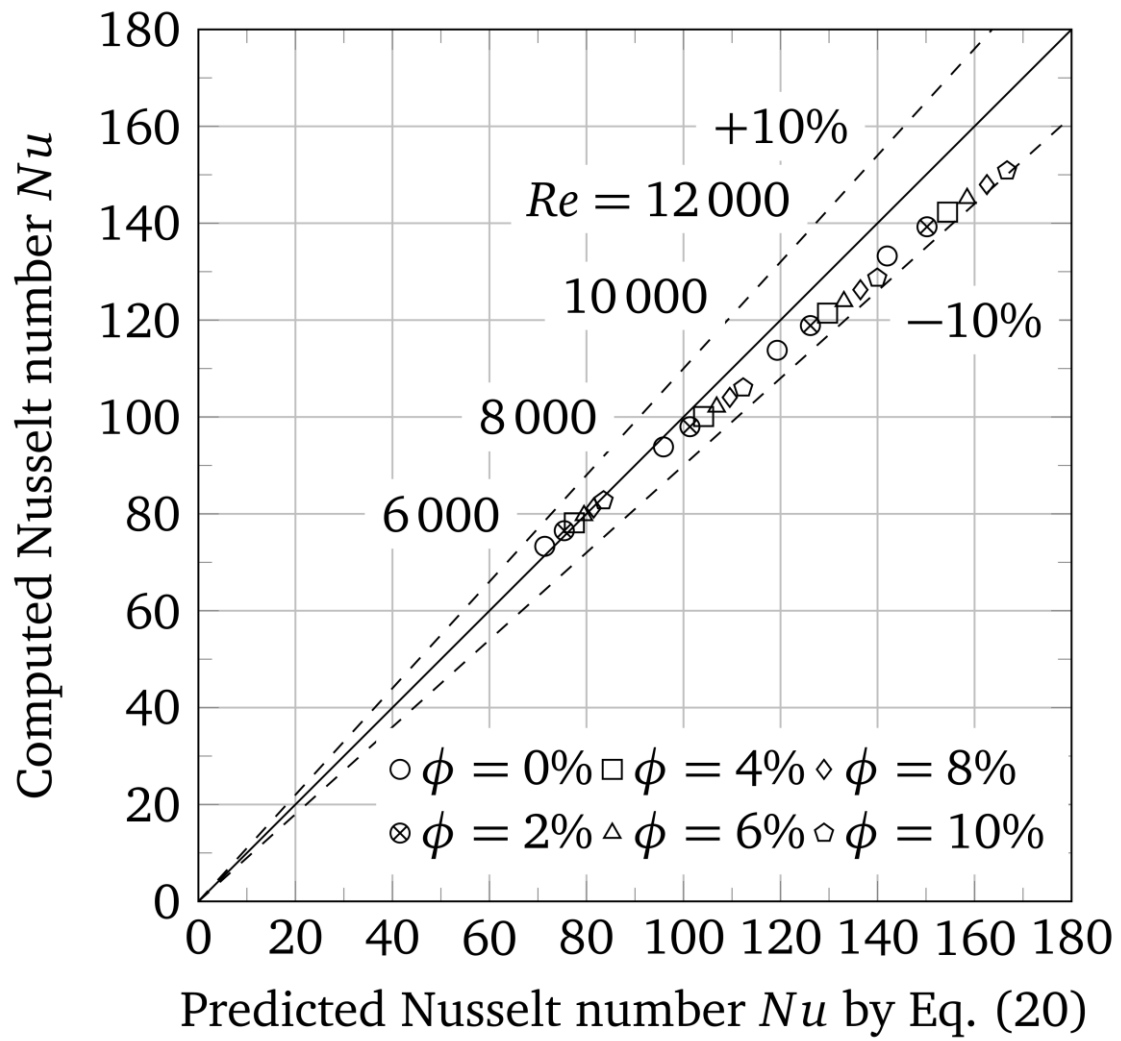
Figure 5 Comparison of the Nusselt number by Gnielinski [43] and computed Nusselt numbers
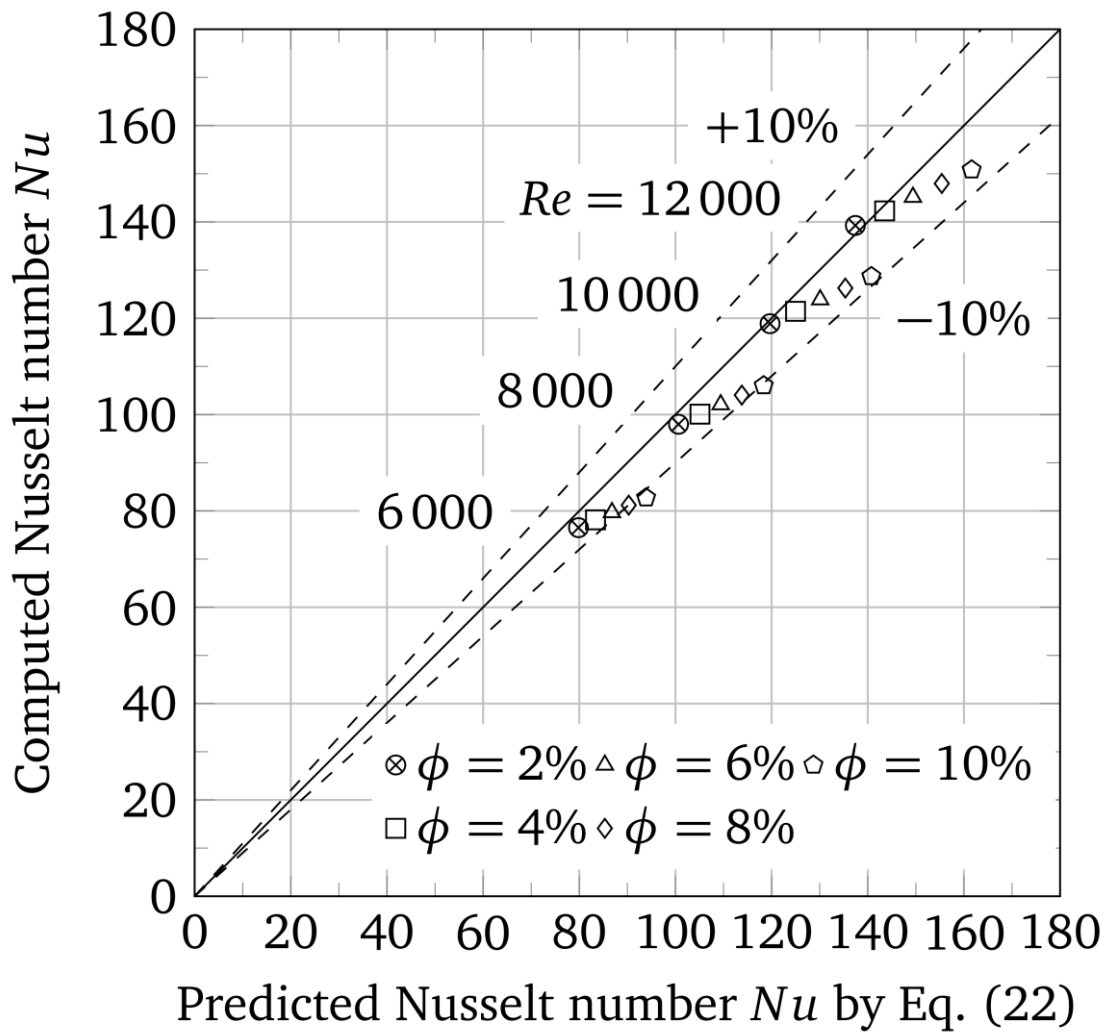
Figure 6 Comparison of experimental Nusselt numbers by Vajjha et al. [25] and computed Nusselt numbers
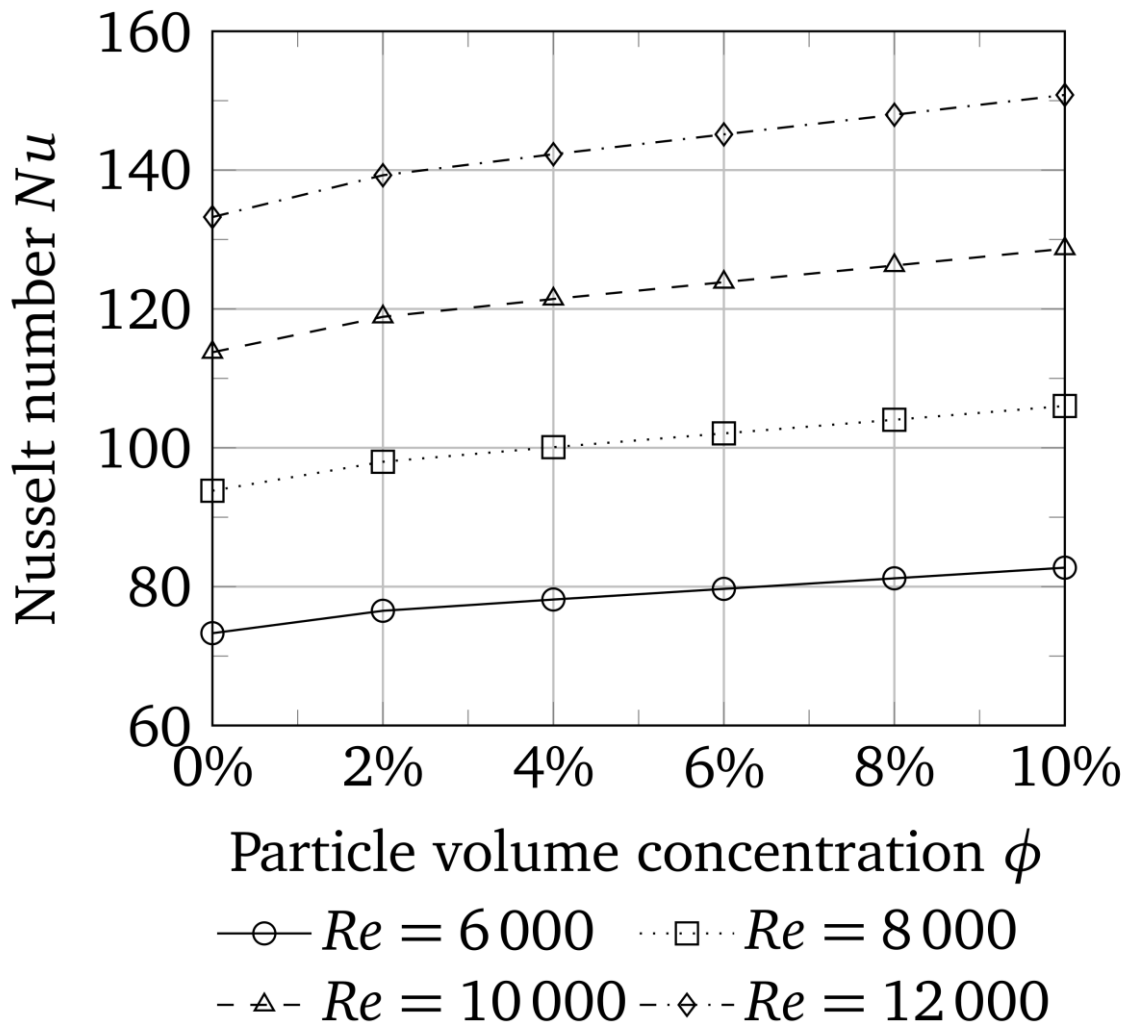
Figure 7 Computed Nusselt numbers of base- and nanofluid

Figure 8 Prandtl number of base- and nanofluid

Figure 9 Pumping power ratio for equal heat transfer of base and nanofluid (Re_{bf}=6000)

Figure 10 Pumping power ratio for equal heat transfer of base- and nanofluid (Re_{bf}=8000)

Figure 1 Schematic diagram of the tube heat exchanger and boundary conditions

Figure 2 Grid example with reduced cell number in z-direction

Figure 3 Comparison of the friction factor by Blasius and computed values

Figure 4 Friction factor for base- and nanofluid (Eqs. 18 and 19) with varying Reynolds number in comparison with computed friction factors

Figure 5 Comparison of the Nusselt number by Gnielinski [43] and computed Nusselt numbers

Figure 6 Comparison of experimental Nusselt numbers by Vajjha et al. [25] and computed Nusselt numbers

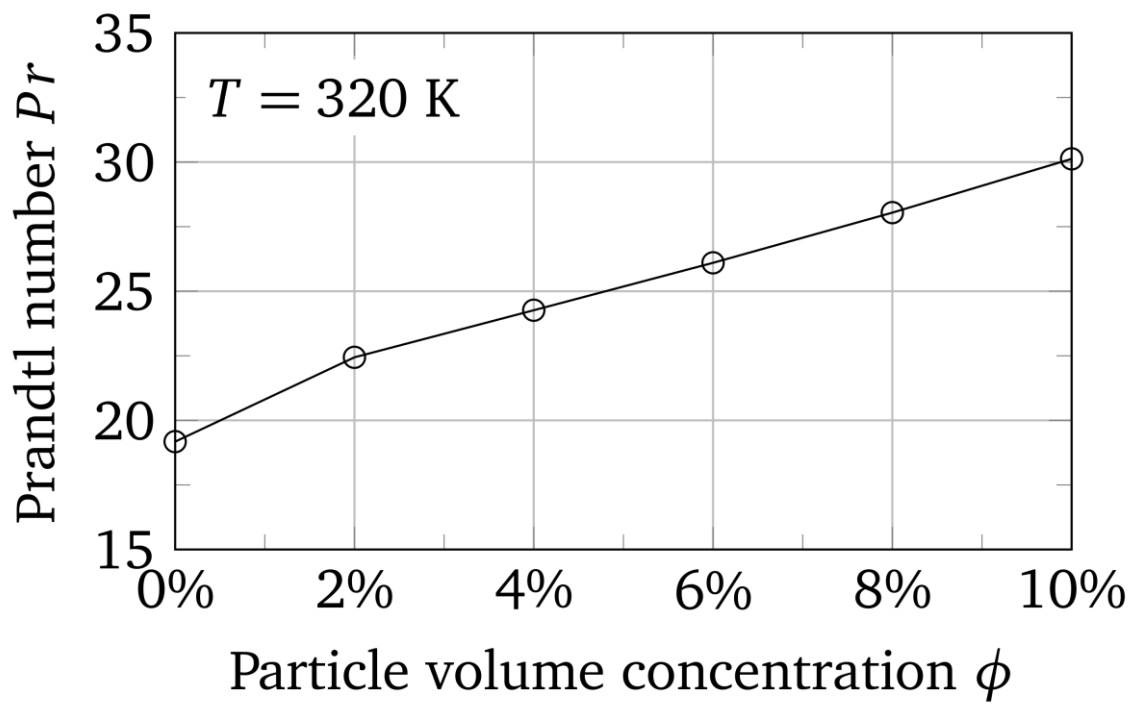**Figure 7 Computed Nusselt numbers of base- and nanofluid**

Figure 8 Prandtl number of base- and nanofluid

$Re_{bf} = 6\,000$

Simulation results

Comparison using Eq. (20) as Nu_{bf}
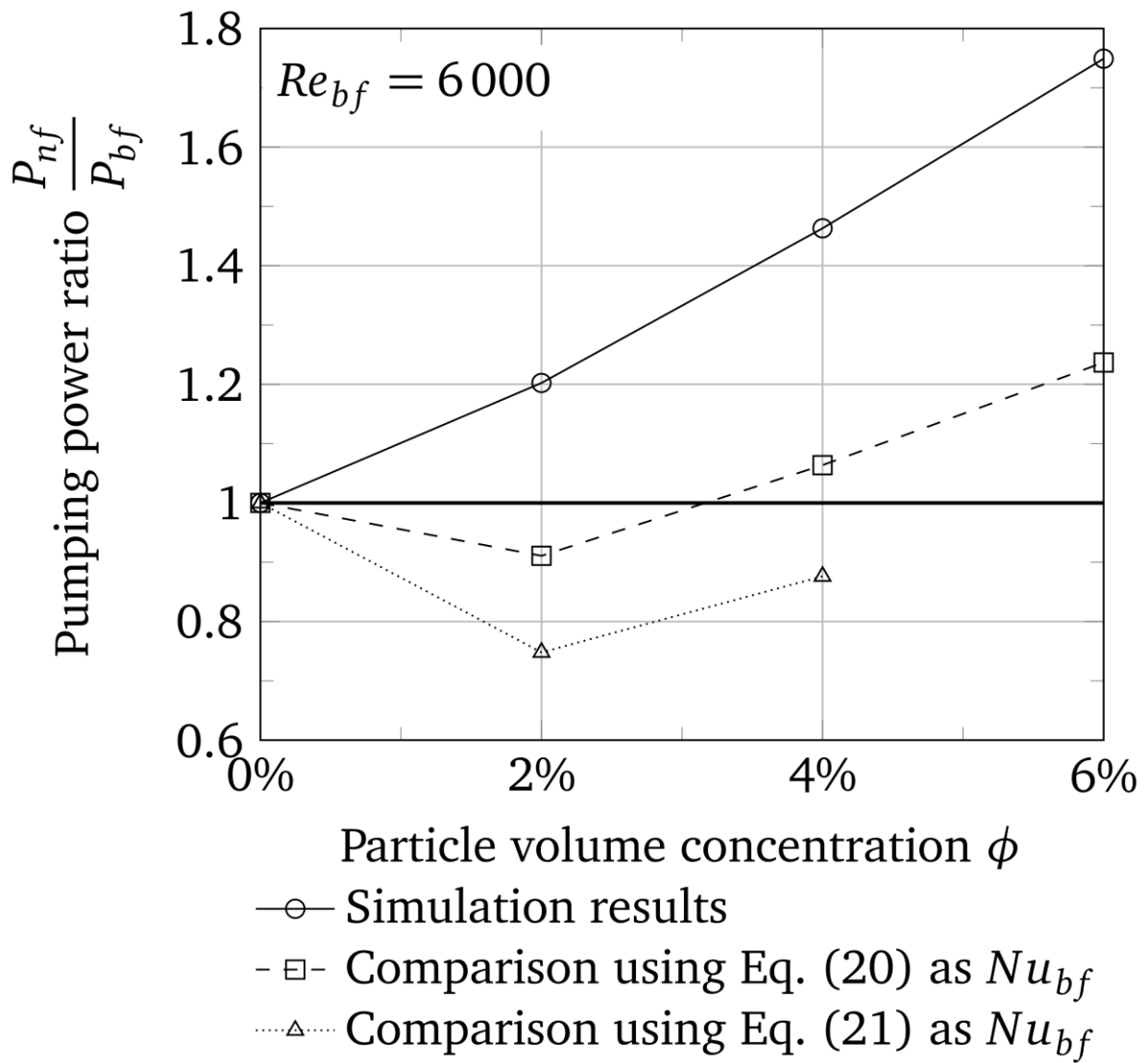
Comparison using Eq. (21) as Nu_{bf}

Figure 9 Pumping power ratio for equal heat transfer of base and nanofluid (Re$_{bf}$=6000)
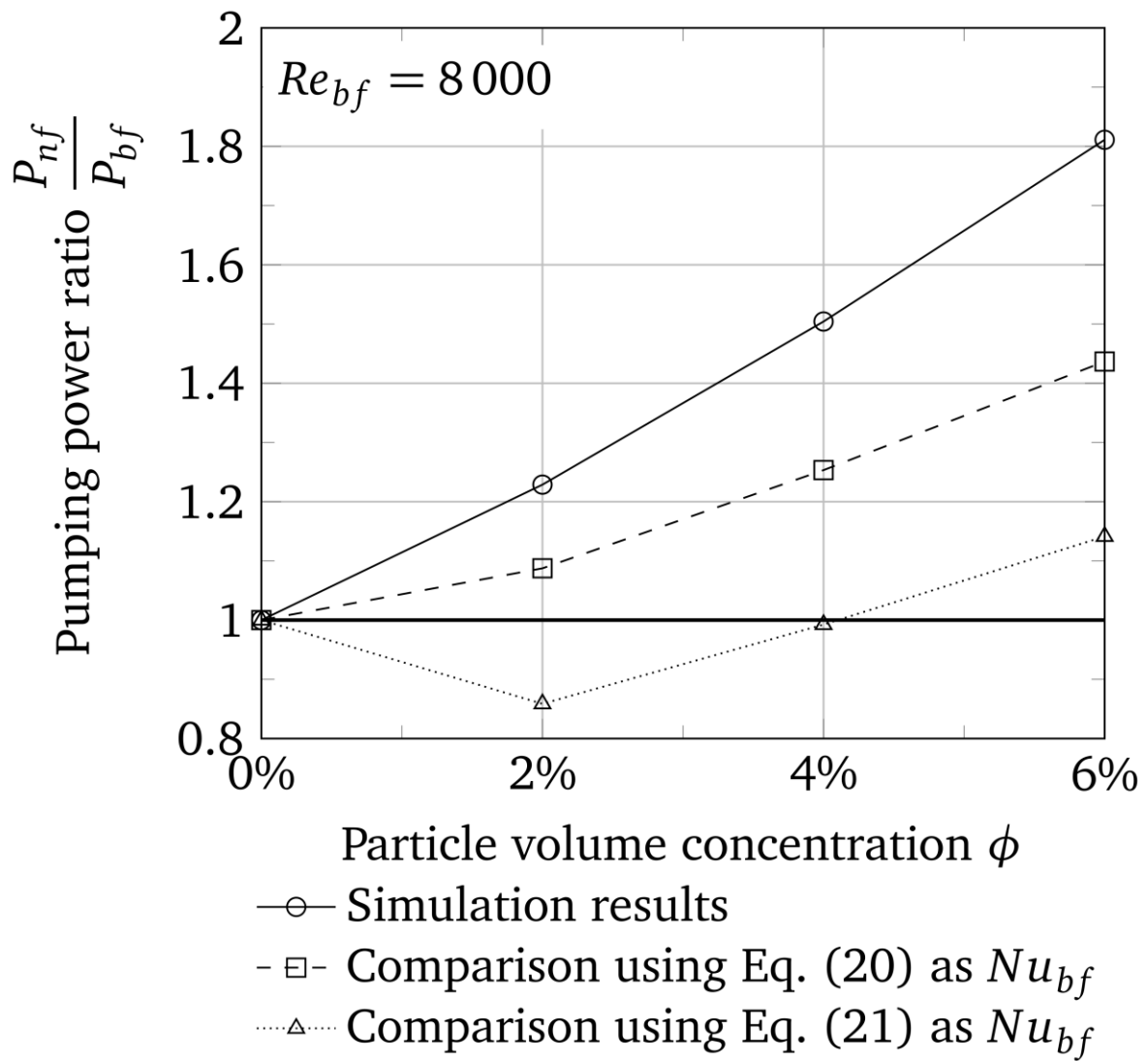
Figure 10 Pumping power ratio for equal heat transfer of base- and nanofluid (Re$_{bf}$=8000)

BIOGRAPHICAL INFORMATION

Hendrik Boertz received his B.Eng. in Energy Engineering from City University of Applied Sciences Bremen in 2014. From 2014 to 2016 he was working as a development engineer for an industrial burner company in Bremen. Since 2016 he studies Energy Engineering (M.Eng.) at University of Applied Sciences Kempten.

Albert J. Baars is professor of fluid dynamics in the department of biomimetics at City University of Applied Sciences Bremen. He received his diploma in mechanical engineering at University of Essen, his PhD at Technical University of Munich and the habilitation at University of Erlangen. His research interests are biological flows using numerical flow simulation.

Janusz T. Cieśliński: He received his MSc degree in Mechanical Engineering from Gdansk University of Technology in 1978 as well as his PhD degree in 1986. He also received his DSc degree (habilitation) from Gdansk University of Technology in 1997. In 2002-2008 he served as a vice dean of the Faculty of Mechanical Engineering. In 2006-2010 he was head of the Chair of Ecoengineering and Process Apparatus and since 2010 he is head of the Ecoengineering and Combustion Engines Division. In 2002-2007 he was a chairman of the Multi-Phase Flow and Non-Newtonian Fluids Section of the Polish Academy of Sciences. Since 2011 he is a member of the Committee of Thermodynamics and Combustion of the Polish Academy of Sciences. Since 2008 he is full professor at Gdansk University of Technology.

Slawomir Smolen is professor and head of institute for Energy Engineering at City University of Applied Sciences Bremen. He received his MSc degree in Mechanical Engineering from Technical University in Szczecin in 1982 and his PhD degree in 1990/1991.

After that he participated in many national and international postdoctoral research projects. In 1996-2000 he worked for Polish and German industrial companies managing projects on the area of energy engineering and energy supply systems. Since 2000 he is professor in Bremen.